

High-frequency photorefractive amplification for ATR applications

Russell M. Kurtz*, Albert O. Okorogu, Judy Piranian, Gilda Fathi, Kang-Bin Chua,
Ranjit D. Pradhan, Thomas C. Forrester, and Tomasz P. Jansson
Physical Optics Corporation, Torrance, CA

ABSTRACT

Automatic target recognition (ATR) can be accomplished by many methods, including recognition of vibrometric signatures. In many cases, ATR is enhanced by photorefractive amplification, a two-wave mixing effect in which two input beams form a dynamic holographic grating. One of the two beams (the pump) diffracts from that grating into the other (the signal), assuming the characteristics of the signal. When the pump is much stronger than the signal, the diffracted pump becomes a highly amplified signal beam. Traditionally, however, the frequency at which this amplification can be applied is limited to $<1/2\pi\tau_0$, where τ_0 is the decay time of the grating in the absence of a pump or signal. We demonstrate that the amplification has no such limit in the case of vibrometry, which measures frequency-modulated, rather than amplitude-modulated, signals. This is shown by constant photorefractive amplification at frequencies up to >700 kHz in Cu:KNSBN, which has $\tau_0 >100$ ms (corresponding to a maximum amplification frequency of 1.6 Hz).

Keywords: High-speed photorefractive effect, photorefractive, KNSBN, automatic target recognition, vibrometry

1. INTRODUCTION

Photorefractivity is a well-known process, with several books and articles published on the subject. The basic equations describing the process were derived by Kukhtarev¹ and published in 1979. The Kukhtarev equations have been applied successfully to descriptions of photorefractivity over the years, and have proven accurate. Yeh² pointed out that, these equations notwithstanding, there is a fundamental limit on the speed of grating formation—it is not possible to photoinduce more carriers than the number of photons absorbed. Indeed, the speed of grating formation is generally much slower than this limit. These equations and analysis of the “dark decay” of photorefractive crystals³ (“dark decay” refers to the decay rate of a photorefractive grating in the absence of writing or erasing beams) indicated that the crystal response time is limited by the dark decay rate τ_0 . This, in turn, led to the conclusion that photorefractive crystals cannot amplify signals (vibrational signals, for example) whose frequencies exceed $1/2\pi\tau_0$.

In this paper, we present the extension of this model to the case of frequency-modulated signals. This includes a preliminary theoretical model as well as experimental results. Our experiments have demonstrated that the response time limitations for *amplitude* modulation (in which the grating must be completely erased and rewritten to amplify the signal) can be overcome for vibrational signals, which exhibit *frequency* or *phase* modulation (i.e., in which the frequency of the signal beam varies with respect to that of the reference beam; see Fig. 1 for definitions).

* Corresponding author: rkurtz@poc.com, phone (310) 320-3088, fax (413) 208-7269

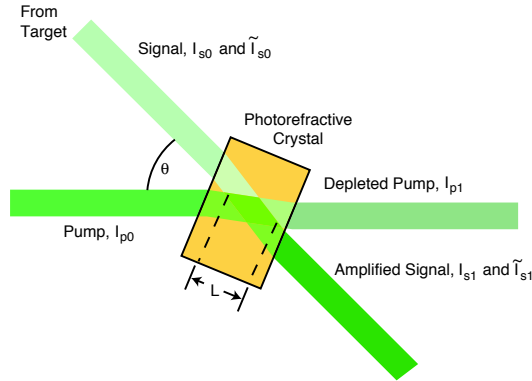


Fig. 1. Layout of a photorefractive experiment, showing the orientations of the signal and reference beams, as well as the interaction angle θ and the interaction length L .

2. BACKGROUND AND THEORY

2.1. Principle of Photorefractivity

Photorefractivity is generally a slow process because it involves a significant rearrangement of space charges in a medium that, for highest efficiency, is characterized by a low value of carrier mobility. The photorefractive material must contain a species (the donor) that has low concentration and can be photoionized at an energy sufficiently low that the host is transparent (Fig. 2). There may be other ions existing as free acceptor sites, or all the acceptor sites may be created by photoionization of donors.

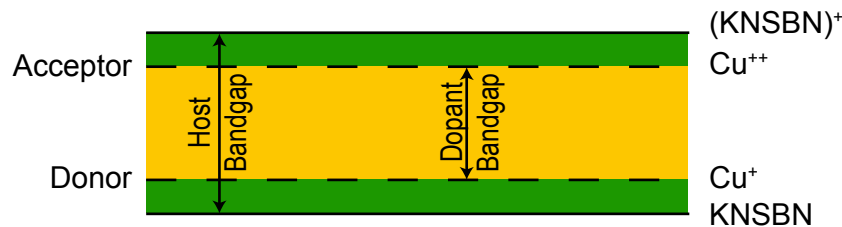


Fig. 2. A typical photorefractive material consists of a low-mobility host, usually a crystalline insulator, doped with a material that has a significantly smaller bandgap. As described below, our experiments used Cu:KNSBN.

When a photon is absorbed by the donor ion, it releases a carrier. If no other processes intervene, this carrier will remain free until, through a process of diffusion, it encounters an acceptor ion. The length of time required for the free carrier to encounter an acceptor is also the dark decay time mentioned above. When setting up a photorefractive experiment, however, the signal and reference beams are assumed to be constant and at the same wavelength (or oscillation frequency). The interaction of the two beams results in a standing wave interference pattern whose spacing is

$$\Lambda = \frac{\lambda}{2 \sin(\theta/2)}, \quad (1)$$

where λ is the wavelength of the reference (or signal) beam. The photogeneration of free carriers is greatest in the area where the light intensity is greatest, but so is the photoinduced recombination. After the carriers are generated, they will drift throughout the host (due to a combination of diffusion, applied electric field, and internal electric field). They recombine rapidly in the areas of high intensity, and thus seem to collect in areas of lower radiation intensity. This process will eventually reach steady state, in which photogeneration of new carriers is exactly matched by recombination due to all causes.

This macroscopic motion of charges results in a large internal electric field with a peak value ~ 10 kV/cm. This internal field creates a refractive index grating through the linear electro-optic effect. Since this grating is created by the

interference of two beams, in the absence of an applied electric field it will be exactly Bragg-matched for reflection for one beam and Bragg-matched for transmission for the other (in Fig. 1 the grating is matched to reflect the pump and transmit the signal). We can now list the four requirements for a good photorefractive material:

1. The host must be transparent at the wavelength of interest.
2. The dopant must be photoionized by radiation at the wavelength of interest.
3. The host must have low carrier mobility.
4. The host must demonstrate a large linear electro-optic effect.

In addition, the doping level of donor ions can be optimized to a level sufficiently low to avoid increasing carrier mobility or saturability of the donor, but sufficiently high to ensure good absorption of the beam and a large internal space charge field once the carriers are saturated.

2.2. Application to Cu:KNSBN

Our experiments used KNSBN [nominally $(K_{0.5}Na_{0.5})_{0.2}(Sr_{0.6}Ba_{0.4})_{0.9}Nb_2O_6$], doped with 0.04% (by weight) Cu^+ . Based on the standard growth ratios of K_2CO_3 , Na_2CO_3 , $SrCO_3$, $BaCO_3$, and Nb_2O_5 , 0.0400 wt % of CuO added to the mixture would result in an atomic doping level of 0.216%, or a concentration of $8.52 \times 10^{18} \text{ cm}^{-3}$. Testing our crystal with the four requirements listed above, we find:

1. KNSBN is transparent at wavelengths $>400 \text{ nm}$.
2. Cu^+ is photoionized at wavelengths $<540 \text{ nm}$.
3. KNSBN is a nearly insulating crystal, with carrier mobility estimated at $<1 \text{ cm}^2/\text{V-s}$.
4. KNSBN has a large linear electro-optic effect, $r_{33} \sim 400 \text{ pm/V}$.

We can thus conclude that Cu:KNSBN will be a good photorefractive material for light in the range $400 \text{ nm} < \lambda < 540 \text{ nm}$. Assuming an angle between the signal and pump beams of $\theta = 45^\circ$, the grating spacing will be 695 nm for illumination at 532 nm , and the saturated maximum internal space charge voltage will be 9.63 kV/cm . Based on the crystal's extraordinary refractive index of 2.53, and the refractive index change calculated from

$$\Delta n = -\frac{1}{2} n_e^3 r_{33} E_z \quad , \quad (2)$$

we find the saturated refractive index variation in the z -direction to be

$$n_z = n_e - 0.00123 \sin\left(\frac{2\pi z}{695 \text{ nm}}\right) \quad . \quad (3)$$

The sinusoidal shape is an approximation; since the field is caused by space charge saturation, it will actually fall between a square wave and a sine wave. Our crystal of Cu:KNSBN was cut along the optical axes, with length 4.0 mm along the x -axis, 5.0 mm along the y , and 6.0 mm along the z -axis. With the two beams angled at $\theta = 45^\circ$ and beam diameters measured as 2.89 mm , the interaction length L is limited by the thickness of the crystal. Depending on crystal orientation, L can be either 3.9 mm or 4.9 mm , while keeping the polarization along the z -axis and taking advantage of the large r_{33} in KNSBN.

2.3. Frequency Response (for Amplitude-Modulated Signals)

The measured value of the decay time of the index grating is $>100 \text{ ms}$ (the grating was being erased by the reference beam; other tests have indicated τ_0 to be several seconds). Using the standard calculation

$$\Delta f \leq \frac{1}{2\pi\tau_0} \quad , \quad (4)$$

the maximum frequency bandwidth is predicted to be 1.6 Hz. Since $\tau_0 > 100$ ms, 1.6 Hz is an upper bound according to standard photorefractive theory.

3. EXPERIMENT

We tested our photorefractive crystal using the experimental setup shown in Fig. 3. A Coherent Verdi V6 frequency-doubled Nd:YVO₄ laser, operating at 532 nm, was the source of both pump and signal beams. We operated the laser at outputs between 200 and 400 mW. The beamsplitter was a glass wedge, with reflectivity that could be adjusted by altering its angle of incidence. The laser was horizontally polarized, so the reflectivity at 45° incidence was 0.93%, with 98% transmitted. The angle between the two beams was set to ~45° by experimentally determining the angle of greatest photorefractive amplification. The modulator was either a NovaPhase EO-PM-NR-C4 (for phase modulation) or EO-AM-NR-C4 (for amplitude modulation). With the EO-HVA amplifier included, the phase modulator was capable of up to $\pm 2\pi$ modulation of a 532-nm signal at up to 2 MHz, while the amplitude modulator could vary transmission between 0 and 100% in < 0.5 μ s. The detectors were Thorlabs FDS010 silicon photodiodes, biased at 9 V, with 1-ns rise times. Data was collected by a Tektronix 3052 digital processing oscilloscope, with a bandwidth of 500 MHz collecting up to 5 GS/s, and output to Microsoft Excel for graphing.

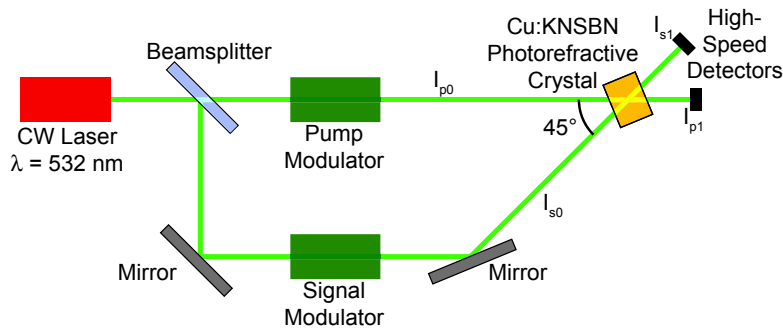


Fig. 3. Photorefractive tests were carried out using a 532-nm laser. The pump modulator was used to transmit or block the pump beam and could switch from 0% to 100% transmission in < 100 μ s.

The first tests were just to demonstrate the photorefractive effect. In these, the modulator was used as a shutter. While the laser output was set to 300 mW (which corresponds to total transmitted power of 220 mW after the crystal), the beam diameter ($1/e^2$ points) was measured at 2.89 mm by a Photon, Inc. USBeamPro beam profiler, so $I_{p1} = 3.29$ W/cm² and $I_{s1} = 0.0312$ W/cm² at the start of each test. In one test, the pump modulator was opened while the signal modulator was closed. After the system reached equilibrium, the signal modulator was opened. Power was immediately transferred from the pump to the signal, with a time constant ~ 1.88 s (Fig. 4(a)). The beams eventually reached equilibrium intensities of $I_{p1} = 0.299$ W/cm² and $I_{s1} = 3.02$ W/cm². Then the roles were reversed. The signal was passed through the crystal, which was allowed to reach equilibrium, and the pump modulator was opened. The transmitted pump nearly reached its maximum potential value before transferring power to the signal with a time constant ~ 0.44 s (Fig. 4(b)). Note that both these time constants significantly exceed the estimated dark decay of ~ 100 ms. Long-term beam intensities of this test matched those of the first test. In both cases, the single-pass photorefractive amplification factor of this setup was 96.8 \times , or 19.9 dB. In this paper, the amplification factor is defined in the photorefractive sense, corrected for reflection and absorption in the crystal. In other words, if $\alpha = I_{s1}/I_{s0}$ in the absence of a pump beam, amplification in the presence of the pump is $I_{s1}/\alpha I_{s0}$. While not equal to the signal amplification, this value is equal to the SNR improvement.

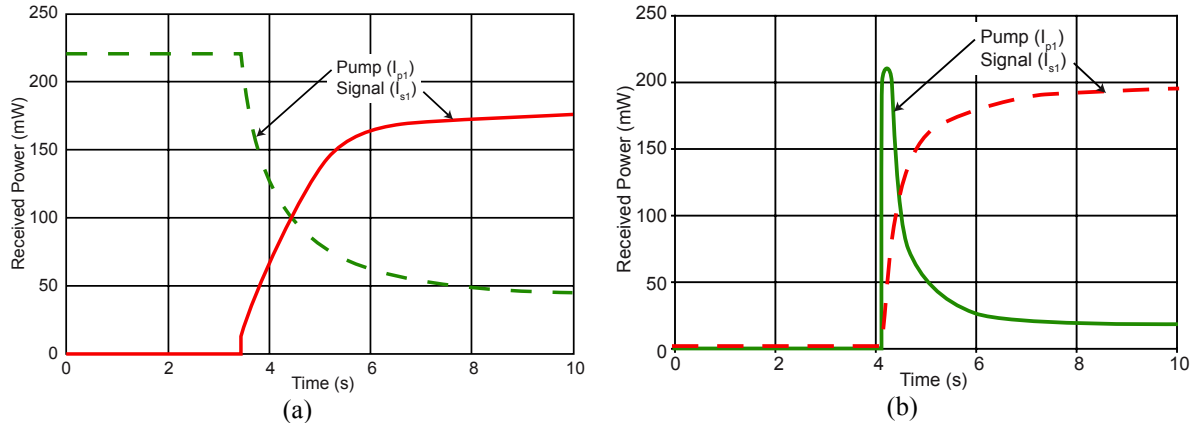


Fig. 4. Tests of the Cu:KNSBN crystal demonstrated the photorefractive effect by transferring power from the pump beam to the signal beam when the signal was turned on in the presence of the pump (a), and when the pump was turned on in the presence of a signal (b).

In the next test, *designed to demonstrate the fast photorefractive effect*, we modulated the phase of the signal beam, while leaving the pump beam untouched. The photorefractive grating reached steady state before the start of signal modulation. We set the signal modulator phase offset and amplitude to act as a nearly perfect frequency shifter, altering the frequency of the signal beam by the phase modulation frequency. Homodyne interferometry demonstrated that there was little fundamental remaining after the shift, and that the frequency sidebands (at $\pm 2 \Delta\nu$, $\pm 3 \Delta\nu$, etc., where $\Delta\nu$ is the frequency of phase modulation) were also very low. In other words, the laser, initially operating at frequency $\nu = c/\lambda$, was now modulated into two beams whose frequencies were $\nu + \Delta\nu$ and $\nu - \Delta\nu$. Using a drive voltage of ± 75 V, 63% of the total signal power was modulated into this first sideband (13% remained in the fundamental and 21% appeared in the second sideband), although the measurements showed virtually no power at any frequency except the first sideband. The DC single-pass amplification was 28 (14 dB). We mixed the amplified beam with $\sim 10\%$ of the pump to act as a homodyne interferometer and specifically measured the signal that was varying at $\Delta\nu$, ensuring that we measured specific amplification for a frequency difference of $\Delta\nu$ between the signal and pump beams. At low frequency the amplification dropped to a factor of 24, varying between 13 and 27 over most of the 1 Hz – 2 MHz range (the frequency limit of the modulator). There are some factors of interest, however. For example, the amplification reached 44 (16 dB) at a frequency of 100 kHz, and nearly the same value at 600 kHz. Amplification was then reduced to 1.2 (0.8 dB) at 800 kHz before rising again to 13 (11 dB) and remaining roughly constant from 1 MHz to 2 MHz (Fig. 5).

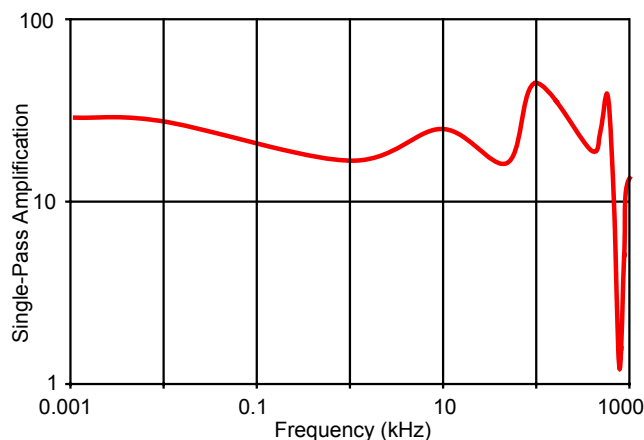


Fig. 5. The Cu:KNSBN photorefractive amplifier had a vibration measurement bandwidth ~ 700 kHz.

This experiment demonstrated that the photorefractive crystal could measure vibration up to a frequency of at least 700 kHz, nearly six orders of magnitude higher than the cutoff frequency predicted theoretically, for amplitude-

modulated signals (Section 2.3). We also tested the photorefractive amplification of signals from lasers at other wavelengths. We replaced the beamsplitter and first mirror in Fig. 3 with independent lasers whose polarization was adjusted to be horizontal, matching the pump laser. The lasers we used were a multimode, doubled Nd:YVO₄ laser operating at 532 nm and a line-selectable HeNe laser with output at 543 nm, 594 nm, 612 nm, and 633 nm. The independent Nd:YVO₄ laser was not measurably coherent with the pump laser, determined by heterodyne interferometry. The pump source was adjusted to $I_{p1} = 265$ mW for all cases. The amplification in each case is shown in Table 1. The amplification values listed include compensation for scattered pump light. Only signal power, not intensity, was measured; this is indicated in the table by a multiplication of the signal intensity by the beam area A.

Table 1. Single-Pass Photorefractive Amplification of Noncoherent Signals.

Laser	Signal $I_{s0}A$	Signal $I_{s1}A$	Amplification
NdYVO ₄ , 532 nm	0.49 mW	0.22 mW	42 (16 dB)
HeNe, 543 nm	0.1 mW	0.04 mW	2.3 (3.7 dB)
HeNe, 594 nm	0.07 mW	0.04 mW	2.4 (3.8 dB)
HeNe, 612 nm	0.48 mW	0.29 mW	1.7 (2.3 dB)
HeNe, 633 nm	0.46 mW	0.31 mW	1.0 (0.0 dB)

Clearly, there is significant amplification for beams with a frequency difference of several GHz, and there appears to be some for signals that are up to 58 THz apart (signal 594 nm, pump 532 nm). But for a sufficient wavelength difference (100 nm, or 89 THz, in this case) there is no amplification.

4. DISCUSSION

Cu:KNSBN has been shown to be an excellent photorefractive material. With a beam intensity ratio of 105 (pump/signal), we achieved 90.8% diffraction efficiency (reflection from the pump into the probe beam), resulting in an amplification of 19.9 dB. This is a quite significant value of amplification.

In a separate experiment, in which the beam intensity ratio was $I_{p0} / \tilde{I}_{s0} \sim 60$, we measured a maximum photorefractive amplification of 44 (70% reflection of the pump into the probe beam), a DC diffraction efficiency of 47% (amplification of 28), and a bandwidth for phase-modulated signals of ~ 700 kHz. This is far beyond the predicted bandwidth, which is based on amplitude-modulated signals. In the amplitude modulation case, the internal electric field must decay and be rebuilt once per period. In phase modulation, the field remains, although it is no longer a stationary field. Most analyses of the photorefractive effect ignore this internal field, and only take account of applied electric fields. In the absence of photovoltaic current, with the illuminating beams aligned such that the interference pattern gradient is along the crystal *c*-axis (which we align with the optical *z*-axis)—the conditions of our experiments—the coupled Kukhtarev equations can be written

$$\frac{\partial n_c^-}{\partial t} = \frac{\partial n_D^+}{\partial t} + \mu_e n_c^- \frac{\partial E}{\partial z} + \frac{\mu_e k T}{e} \left[\left(\frac{1}{n_c^-} \frac{\partial n_c^-}{\partial z} \right)^2 - \frac{\partial^2 n_c^-}{\partial z^2} \right], \quad (5)$$

and

$$\frac{\partial n_D^+}{\partial t} = (\sigma I + \beta)(n_D - n_D^+) - \frac{n_c^- n_D^+}{\tau_R}, \quad (6)$$

(under the assumption that the *z*-directed internal electric field does not generate *x*- or *y*-directed effects—generally true of KNSBN), where n_D is the total density of possible donors (Cu⁺ and Cu⁺⁺), n_D^+ is the density of ionized donors (Cu⁺⁺), n_c^- is the density of free carriers (electrons), $\vec{E}(x, y, z)$ is the total internal electric field, μ_e is the free carrier mobility, k is Boltzmann's constant, T is the absolute temperature, e is the charge of an electron, σ is the photoionization cross-section, I is the light intensity (so σI is the rate of photoionization), β is the thermal ionization rate, and τ_R is the dark recombination time. Partial derivatives have been used to emphasize the fact that E and n_c^- may be functions of time as well as space. In fact, the electric field $\vec{E}(x, y, z)$ is a result of the charge distribution $n_c^-(x, y, z)$, and follows the same form, driven by the intensity of the interfering beams,

$$I(z) = (I_{s0} + I_{p0})(1 - R) \left[1 + \frac{\sqrt{I_{s0}I_{p0}}}{I_{s0} + I_{p0}} \cos \theta \sin \left(\frac{2\pi z}{\Lambda} + \varphi \right) \right], \quad (7)$$

where the parameters are defined in Fig. 1 and Eq. (1), with the exception of φ , an arbitrary phase, and R , the Fresnel reflectivity of the crystal at incidence angle $\theta/2$. When this interference pattern forms a standing wave, that is, when the pump and signal beams are at the same frequency, the carrier density rapidly saturates and produces a steady-state electric field grating. This grating has the same period Λ as the driving intensity interference pattern in Eq. (7), although the phase is different. The carrier density distribution results in an electric field pattern which, through the first-order electro-optic effect, induces an index grating whose form falls between a sinusoid and a square wave. Analyzing Eqs. (5) and (6) we see that, as long as the intensity interference pattern is sufficient to overcome thermal carrier generation, that is, as long as

$$(I_{s0} + I_{p0})(1 - R) \frac{\sqrt{I_{s0}I_{p0}}}{I_{s0} + I_{p0}} \cos \theta > \beta, \quad (8)$$

the carrier density will eventually saturate at

$$n_c^- = \frac{n_D^- - n_D^+}{n_D^+} (\sigma I - \beta) \tau_R, \quad (9)$$

which, since n_D^+ depends on I , is nearly constant with I . Since the electric field results from the space-charge distribution, the diffraction efficiency of the steady-state photorefractive effect is not strongly dependent on the intensity of the illumination.

When the illumination intensity is time-dependent, the space charge distribution will also be time-dependent, as will the internal electric field. If the variation in intensity is macroscopic, as in amplitude modulation, the entire space charge distribution must change significantly. Solving Eqs. (5) and (6) under these conditions indicates that there is a long delay (roughly inversely proportional to I) between such a macroscopic change and the resulting change in the distribution of free carriers. On the other hand, a change over microscopic distances—such as the temporal variation of intensity resulting from a “moving grating,” caused by different center frequencies of the pump and signal beams—is a perturbation rather than a complete realignment of space charges. Since the macroscopic charge distribution (over distances $> \Lambda$) is not changing, large space charge distributions do not occur, and nor does the traditional frequency limit of $1/2\pi\tau_0$. Another way to look at this is to consider the motion of the charges inside the crystal. When there is a macroscopic change, free carriers must be moved from one location to another, inducing a macroscopic change in the electric field. The ultimate example of this is when the pump and signal beams first illuminate the photorefractive material. This is a slow effect, since the speed of motion of the free carriers is limited to the mobility multiplied by the electric field (and estimates of the mobility in Cu:KNSBN are small, in most cases $< 1 \text{ cm}^2/\text{V}\cdot\text{s}$). When there is virtually no field, or just the applied field of the illumination ($\sim 50 \text{ V/cm}$), the velocity of carrier motion is very slow. Under photorefractive conditions, however, the internal electric field due to space charge reorientation is up to 10 kV/cm , increasing the potential speed of charge motion by a factor of 200. In addition, if there is a difference between the center frequencies of the pump and signal, the value of I in Eq. (6) varies with time, forcing a nonzero value for $\partial n_c^- / \partial t$. Finally, in the cases of phase modulation and frequency modulation, there is a large concentration of free carriers at the start of the variation, while in the traditional method of measuring τ_0 , there are no free carriers when the beams are initiated. We speculate that the combination of these three effects results in a much faster time response of the free carrier density than is found by measuring dark decay or turn-on rate, and that this explains the nearly constant value of photorefractive amplification from DC to 700 kHz in our experiment.

Analysis of the experiment using separate lasers demonstrates another interesting point. We found that the amplification of a multimode laser nominally operating at the same wavelength as the pump, although not coherent with it and with a center frequency so far separated that the moving interference pattern could not be detected, was amplified nearly as much as a signal that was fully coherent with the pump. A signal whose center frequency was separated by nearly

60 THz from the pump was slightly amplified, while signals >90 THz away from the pump center frequency were not amplified. Note that the “amplification” appeared as light at 532 nm being diffracted into the same direction as the signal beam; the signal was not amplified at its own wavelength. This amplification is an effect of the nonzero linewidth of the lasers. The pump laser had a Lorentzian linewidth, which theoretically has finite values at very large frequencies; the HeNe signals had Gaussian linewidths, which are also theoretically infinite. In practice, the value at the separated frequency is very small. For example, the pump laser had a linewidth of 5 MHz; its normalized value at 594 nm was 2.4×10^{-15} . This is still much larger than the value of the 594-nm HeNe laser at 532 nm. Since $I_{s0}/I_{p0} \sim 4000$, we can calculate $I_{s0}(594 \text{ nm})/I_{p0}(594 \text{ nm}) \sim 9.0 \times 10^{-12}$. Based on an amplification of 2.3, insertion of this ratio into Eq. (8) gives a photoionization rate that is near the thermal carrier generation rate. In other words, even for two independent lasers separated by 62 nm, there was sufficient mutual coherence to generate a very small photorefractive effect. Clearly, the overlap between the laser spectra of the pump and independent 532-nm signal beams was sufficient for full photorefractive amplification.

5. SUMMARY AND CONCLUSIONS

We have studied the photorefractive effect in KNSBN nominally doped with 0.04 wt.% of Cu^+ . In this material, we measured dark decay >100 ms, and as long as 1800 ms (see Fig. 4). Despite this value for τ_0 , we demonstrated photorefractive amplification with a 3-dB bandwidth of ~ 700 kHz and a measurable amplification bandwidth of ~ 60 THz. These values, however, were for frequency shifts rather than amplitude modulation (which is the method used to measure dark decay). We have speculated on the basis of this increased bandwidth, but have not conclusively determined its cause.

The wide bandwidth, however, is useful in vibrometry, since vibrational signatures often include ultrasonic frequencies. The vibrational signatures, in turn, can be used for automatic target recognition. Despite the width of amplification, it should be noted that the ratio of bandwidth to base frequency is small. A 700-kHz bandwidth amplifier operating at 532 nm (563 THz) has a ratio $\Delta\nu/\nu = 1.2 \times 10^{-9}$, effectively a delta function amplification. Thus, use of photorefractive amplification effectively amplifies only the signal at the pump wavelength, and *not the background*. In our tests with amplification of $\sim 100\times$, for example, the signal-to-noise ratio (SNR) of the amplified signal would also be increased by the same factor. Note that this value is the photorefractive amplification or SNR improvement, and is greater than the signal amplification by the factor 1/2 from Section 3. This has significant potential for ATR, vibrometry, and signal processing and switching applications.

6. REFERENCES

1. N.V. Kukhtarev, V.B. Markov, S.G. Odulov, M.S. Soskin, and V.L. Vinetskii, “Holographic Storage in Electrooptic Crystals. II. Beam Coupling—Light Amplification,” *Ferroelectrics*, **22**, 961-964, 1979.
2. P. Yeh, “Fundamental Limit of the Speed of Photorefractive Effect and Its Impact on Device Applications and Material Research,” *Appl. Opt.*, **26**, 602-604, 1987.
3. P. Vaveliuk, B. Ruiz, R. Duchowicz, and N. Bolognini, “Theoretical Analysis of the Photocurrent Dark Decay in Photorefractive Media,” *IEEE J. Quantum Electron.*, **36**, 692-697, 2000.
4. N.V. Kukhtarev, V.B. Markov, S.G. Odulov, M.S. Soskin, and V.L. Vinetskii, “Holographic Storage in Electrooptic Crystals. I. Steady State,” *Ferroelectrics*, **22**, 949-960, 1979.